Available online at www.sciencedirect.com
SCIENCE DIRECT
ELSEVIER
Polymer 46 (2005) 6182–6191
polymer
www.elsevier.com/locate/polymer

Composition effects on the mechanical properties of microemulsion-made core/shell polymers

M. Rabelero[a,*], S. López-Cuenca[a], M. Puca[a], E. Mendizábal[a], J. Esquena[b], C. Solans[b], R.G. López[c], J.E. Puig[a]

[a]*Departamentos de Ingeniería Química y Química, Universidad de Guadalajara, Boul. M. García Barragán # 1451, Guadalajara, Jal. 44430, México*
[b]*Instituto de Investigaciones Químicas y Ambientales de Barcelona, Jordi Girona 18-26, Barcelona 08034, España*
[c]*Centro de Investigación en Química Aplicada, Boul. Ing. Enrique Reyna # 140, Saltillo, Coah. 25100, México*

Received 22 December 2004; received in revised form 23 April 2005; accepted 30 April 2005
Available online 20 June 2005

Abstract

The synthesis of hard-core/soft-shell and soft-core/hard-shell polymers by a two-stage semi-continuous microemulsion polymerization process is reported here. In the first stage, high-solid polymer seeds (>30 wt%) of slightly crosslinked polystyrene or poly(butyl acrylate) were obtained; then, the other monomer was added semi-continuously to form the shell. The effects on the mechanical properties (Young's modulus, ultimate properties, hardness and impact energy) of the ratio of rigid-to-soft and soft-to-rigid polymers were studied. It was found that the material becomes stiffer and presents a lower elongation at break as the amount of the rigid polymer increases. The mechanical properties also depend on the location of the hard and soft polymers. Experimental mechanical properties were compared with the predictions of the Kerner and the equivalent box models. Comparison with the predictions of the Kerner model suggests that phase inversion occurred in the case of hard-core/soft-shell materials. Phase inversion was corroborated by transmission electron microscopy. The thermodynamically preferred morphology, according to theory, is that of soft-core/hard-shell, regardless of the order of addition of monomers. Experimental data follow closely the predictions of the equivalent box model only for soft-core/hard-shell polymers.

Keywords: Microemulsion; Core/shell; Mechanical properties

1. Introduction

Core/shell polymers typically consist of at least two main polymeric domains: one usually having a low-glass transition temperature (T_g) and another with a high-T_g, which are chosen to be lower and higher, respectively, than the working temperature [1–3]. Core/shell polymer particles can be used in a wide range of applications because they exhibit tunable and/or improved chemical and mechanical properties compared to those of the parent-component polymers [4,5]. Core/shell particles differing in glass transition temperatures are used in coatings and non-porous homogeneous films [6–8], as modifiers of the mechanical properties of thermoplastics [9–12] and in the manufacture of nanocomposite materials [13,14]. Typically, a two-stage emulsion polymerization process is used to produce core/shell polymers [3,6,7,11] but also emulsion blending has been employed [15].

Microemulsion polymerization is an alternative process for producing core/shell polymer particles of nanosize scale [16]. In this process, latexes containing tiny particles (<50 nm), each composed of a few macromolecules of high molecular weight (>10^6 Da), are produced [17–20], over which other(s) monomer(s) can be added in batch or semi-continuously to form the shell [16]. However, the low polymer content and the large amount of surfactant required in microemulsion polymerization have hindered its scale up to industrial level [21]. Efforts to overcome this drawback have been reported recently; latexes of polystyrene, poly(butyl acrylate) and other acrylic or vinyl polymers can be produced with high solid content (>30 wt%), without altering the basic features of the microemulsion-made polymer nanoparticles [22–26].

Elsewhere we reported the synthesis of core/shell

* Corresponding author. Tel.: +52 33 3650 3401; fax: 52 33 3619 7316.
E-mail address: mrabelero@hotmail.com (M. Rabelero).

0032-3861/$ - see front matter © 2005 Published by Elsevier Ltd.
doi:10.1016/j.polymer.2005.04.100

polymer particles of nanosize scale by a two-stage microemulsion polymerization process; these materials had better mechanical properties than those of core/shell polymers of similar composition and core/shell ratio made by emulsion polymerization [16]. In this work we report the synthesis by microemulsion polymerization and the mechanical properties of hard-core/soft-shell and soft-core/hard-shell polymers as a function of the ratio of the two forming polymers—poly(butyl acrylate) and polystyrene. The seed latexes were made by adding more monomer in a semi-continuous fashion to increase the solid content. Then the second monomer was also added semi-continuously to form the shell. The mechanical properties (stress–strain, hardness and impact tests) are reported and compared with predictions of the equivalent box and the Kerner models.

2. Experimental

Dodecyltrimethylammonium bromide (DTAB), 99% pure from Tokyo Kasei, was used as received. Styrene (St) and butyl acrylate (BA) were 99% pure from Aldrich. The inhibitors were removed from these monomers by passing them through a DHR-7 or DHR-4 silica gel column (SPP). Allyl methacrylate (ALMA) from Aldrich was used as a crosslinking agent as received. The initiator, 2,2′-azobis (2-amidinopropane) hydrochloride (V-50) from Wako, was re-crystallized from methanol. Water was doubly distilled and de-ionized.

A two-stage semi-continuous microemulsion polymerization process was used for the synthesis of the core/shell polymers. First, microemulsions containing 14.1 wt% DTAB, 79.9 wt% H_2O and 6 wt% styrene or butyl acrylate were polymerized at 60 °C with V-50 ($w_{V\text{-}50}/w_{monomer}=0.01$) in the presence of small amounts of ALMA ($w_{ALMA}/w_{monomer}=0.01$) to produce slightly crosslinked particles. To increase the solid content in the latexes, more monomer was added semi-continuously for over 6 h under monomer-starved conditions. With this technique, the solid content was increased from 5.5 to 36 wt%. After completion of the reaction, the high solid-content latex is diluted with water to 10% solids and used as the seed in the second stage. The required amount of BA (or St) to obtain the desired composition was added semi-continuously in the second stage to form the shell. Then, the core/shell polymer was precipitated by adding excess methanol, filtered, washed to eliminate adsorbed surfactant, and dried in a vacuum oven.

Glass transition temperatures (T_g) were obtained from the second run thermogram, i.e. after one heating-and-cooling scan to eliminate thermal history, with a DSC-7 Perkin–Elmer differential scanning calorimeter at cooling and heating rates of 10 °C.

Particle size was measured with a Malvern 4700C QLS apparatus at room temperature. Intensity correlation data were analyzed by the method of cumulants to provide the average decay rate, $\langle\Gamma\rangle$, ($=2q^2D$, where D is the diffusion coefficient and q is the modulus of the scattering vector). The measured diffusion coefficients were represented in terms of the apparent radii using Stokes law and the assumption that the solvent has the viscosity of water. Lattices were diluted up to 1000 times before QLS measurements to minimize particle–particle interactions.

The microstructures of the composite latex particles were examined in a JEOL 1010 electron transmission microscope at an accelerating voltage of 100 kV. To improve the contrast, samples were treated with a 1% phosphotungstic acid solution for two hours, deposited on copper grids and allowed to dry at room temperature for 24 h before TEM examination.

Polymer bars ($10\times63\times2$ mm^3) for the tensile tests were made by heating at 120 °C and pressing at 150 bars in a hydraulic press. Tensile tests were performed at room temperature according to the ASTM D-638 method at an elongation velocity of 2 in./min in an universal testing machine from United. Shore hardness 'A' was measured according to the ASTM D2240 method with a 306 L PTC instrument. Impact tests were performed according to the ASTM D-1709 method in a CS-126G custom scientific instrument. The dart employed to test the PSt-rich samples weighed 285 g while that used for the PBA-rich probes weighed 920 g. Tensile, hardness and impact data are the average of at least three independent measurements.

3. Results and discussion

Table 1 reports the conversions at the end of stages 1 and 2 for the hard-core/soft-shell and soft-core/hard-shell polymers studied here. Independently of the monomer used to form the seeds and the core/shell composition, final conversions at the first and second stages are high (>90%).

Core/shell polymers with different shell thickness can be made by varying the ratio of shell monomer to core polymer [27]. Table 2 reports % solids and the QLS z-average particle size in stages 1 and 2 for the different core/shell polymer formulations prepared here. At the end of the first stage, all the latexes had a solid content higher than 30% and contain particles of about 42–47 nm in diameter (D_{core}); this

Table 1
Conversions obtained at the end of stages 1 and 2 for the different core/shell formulations

Core/shell composition	Conversion (%) stage 1	Conversion (%) stage 2
PSt/PBA 70/30	94.3	98.9
PSt/PBA 60/40	94.3	94.8
PSt/PBA 50/50	93.8	99.7
PSt/PBA 40/60	93.8	94.3
PBA/PSt 70/30	96.0	94.1
PBA/PSt 60/40	96.0	96.3
PBA/PSt 50/50	96.0	90.6
PBA/PSt 40/60	96.0	90.7

Table 2
Solid content and average particle size at the end of stages 1 and 2, and volume fraction of polymer formed during the second stage, for the core-shell polymers prepared by microemulsion polymerization

Core/shell composition	% Solids stage 1	Dp_z (nm) stage 1	% Solids stage 2	Dp_z (nm)[a] stage 2	Dp_z (nm)[b] stage 2	ϕ^c	ϕ^d
PSt/PBA 70/30	32.4	42.0	15.0	45.3	47.7	0.203	0.317
PSt/PBA 60/40	32.4	42.0	16.3	45.8	49.5	0.229	0.389
PSt/PBA 50/50	39.2	47.3	19.8	58.2	60.6	0.463	0.525
PSt/PBA 40/60	39.2	47.3	22.7	59.2	63.9	0.49	0.594
PBA/PSt 70/30	39.0	41.7	14.5	46.9	47.0	0.297	0.30
PBA/PSt 60/40	39.0	41.7	16.9	49.9	50.1	0.416	0.423
PBA/PSt 50/50	39.0	41.7	18.3	51.2	51.8	0.458	0.478
PBA/PSt 40/60	39.0	41.7	19.3	53.8	56.6	0.534	0.6

[a] Measured by QLS.
[b] Estimated with Eq. (3).
[c] Estimated with actual diameter.
[d] Estimated with expected diameter.

particle size is characteristic of microemulsion polymerization [17,21]. Table 2 also shows that at the end of the second stage, particle size has increased but it remains within the range of microemulsion-made particle size. This growth suggests that the monomer added during the second stage polymerizes over the seed particles to form a core-shell structure. However, this growth does not exclude the formation of other morphologies or additional particles of homo-polymer. To estimate the amount of the second monomer incorporated over the seeds, we compared the z-average particle size with a theoretical value, estimated by knowing the amount of monomer added in the second stage (w_{shell}), the conversion, and the density of the polymer forming presumably the shell (ρ_{shell}), with the assumptions that all the particles (N_{core}) at the end of the first stage have the same size and that the polymer formed in the second stage is uniformly distributed among the particles. The mass balance equations employed to estimate the theoretical size of the core-shell particles are the following:

$$N_{core/shell} = N_{core} = \frac{w_{core}/\rho_{core}}{\pi D_{core}^3/6} \quad (1)$$

$$\frac{w_{shell}}{\rho_{shell}} = \frac{1}{6}\pi N_{core/shell}(D_{core/shell}^3 - D_{core}^3) \quad (2)$$

$$D_{core/shell} = D_{core}\left[\frac{w_{shell}/\rho_{shell}}{w_{core}/\rho_{core}}\right]^{1/3} \quad (3)$$

where w_{core} is the total polymer mass in the core and $D_{core/shell}$ is the final particle diameter.

Within the experimental error and the considerations made, calculated and measured average particle diameters are fairly close in most cases (Table 2), indicating that most of the monomer added in the second stage is incorporated over the seed particles. The actual volume fraction—based on the polymer produced in the second stage, was calculated from the measured particle diameters at the end of the first and second stages. The actual and the expected volume fractions are reported in Table 2. In what follows, we will use the actual polymer volume fraction (ϕ_2). Since, latexes with 10% solids were used in all cases, core/shell lattices with 14–23% solids were obtained depending on the amount of the second monomer added to obtain the desired composition (Table 2). All the latexes were stable for months indicating that it is possible to obtain microemulsion-made structured polymers latexes with high solid content with this procedure.

DSC detected two glass transition temperatures, which is an indication of the presence of two segregated polymer phases in the material. The glass transition temperatures of the core/shell polymers with different compositions are reported in Table 3. Clearly, the lower transition temperature at ca. −50 °C corresponds to poly(butyl acrylate) whereas the higher one (100 °C) corresponds to the T_g of polystyrene. The particle growth and the presence of two polymer phases suggest that a core-shell structure was obtained.

Fig. 1 shows the stress–strain curves of PBA-core/PSt-shell polymers of different compositions as well as that for polystyrene made by microemulsion polymerization. An amplification of the low deformation region is shown in the inset. As expected, the sample with highest PSt content (PBA/PSt = 40/60) is rigid and breaks before yielding, with a smaller tensile stress at break (ca. 10 MPa) than polystyrene (36 MPa), but a slightly larger elongation at break (inset in Fig. 1). The sample with 50/50 weight ratio is

Table 3
Glass transition temperatures of core-shell polymers with different compositions

Core/shell composition	T_{g1} (°C)	T_{g2} (°C)
PSt/PBA 60/40	−45.9	96.6
PSt/PBA 50/50	−48.0	99.3
PSt/PBA 40/60	−52.0	101.4
PBA/PSt 70/30	−51.2	95.1
PBA/PSt 60/40	−51.4	93.8
PBA/PSt 50/50	−53.3	101.5
PBA/PSt 40/60	−55.1	98.7

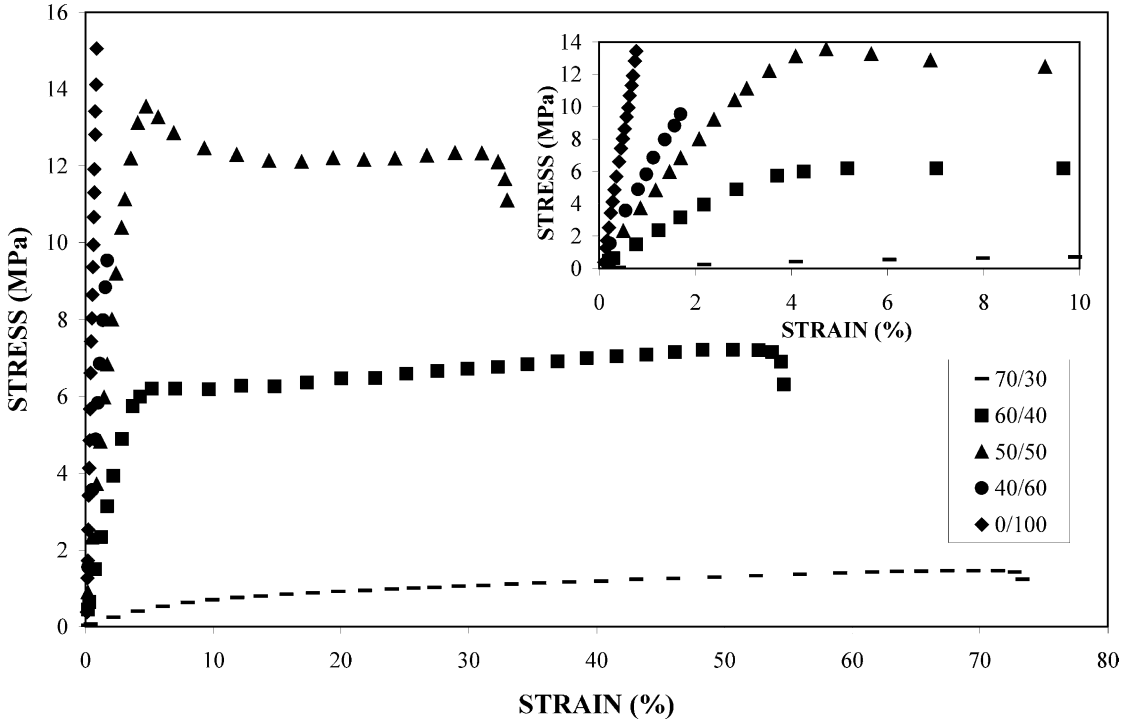

Fig. 1. Stress–strain data for PBA-core/PSt-shell polymers of different PBA/PSt ratios.

rigid but also tough; it yields at about 13.6 MPa and then it exhibits stress softening up to failure. The elongation at break of this sample is almost 20 times larger than that of the 40/60. As the concentration of PSt decreases, the soft-core/hard-shell samples become softer and more elastic. The yielding point decreases to ca. 6 MPa for the 60/40-sample and to ca. 1 MPa for the 70/30-sample, whereas the elongation at break increases from 53 to 75% for these samples, respectively. Hence, the behavior changes from rigid to elastic upon increasing the amount of PBA in the core.

Fig. 2 depicts the stress–strain curves of the PSt-core/PBA-shell polymers of different compositions. Also, the stress–strain response of poly(butyl acylate) made by microemulsion polymerization is reported in this figure for comparison. The sample with PSt/PBA = 40/60 has an elastic behavior with a yield stress at ca. 0.8 MPa and an elongation at break of 150%. Samples with 50/50 and 60/40 exhibit a yield point (inset of Fig. 2) followed by a small region of elongation at constant stress and then stress softening with ultimate stress values much lower than their corresponding yield stresses. The sample with highest PSt content (70/30) is rigid and breaks at a stress of 15 MPa. Fig. 3 reports the tensile modulus versus PSt composition for hard-core/soft-shell and soft-shell/hard-core polymers. Consistently, the polymers with the hard-shell exhibit higher modulus at all compositions due to the rigid nature of the 'continuous phase'. The predictions of the equivalent box model (EBM), which has proven useful to predict the tensile strength and tensile modulus of emulsion polymer blends of high- and low-compliance constituents [15], are also reported in Fig. 3 as a solid line. This model, which is a combination of parallel and series contributions [28,29], gives the following equation for yield and/or tensile strength of a binary blend:

$$\sigma_b = (\sigma_1\phi_{p1} + \sigma_2\phi_{p2}) + A\sigma_{smaller}\phi_s \quad (4)$$

where σ_b, σ_1, σ_2 and are the tensile strengths of the blend and components 1 and 2, respectively, $\sigma_{smaller}$ is the smaller of σ_1 and σ_2, ϕ_{p1} and ϕ_{p2} are the parallel contribution of components 1 and 2 to the volume fraction, $\phi_s(=\phi_{s1}+\phi_{s2})$ is the total series volume fraction contribution and A is the interfacial adhesion, which has two limiting values: 0 for no adhesion and 1 for perfect interfacial adhesion. The volume fraction contributions of the EBM can be calculated by means of the percolation theory for the tensile modulus of a two-component blend with a negligible contribution of the second component; this theory predicts that [30]:

$$E = E_0(\phi - \phi_{PT})^{\beta} \quad (5)$$

where E_0 is a constant, ϕ_{PT} is the percolation threshold volume fraction (=0.156 for discrete spherical domains [30,31]) and β is the critical universal exponent (=1.833 for discrete spherical domains [30,31]). Lyngaae-Jorgersen et al. [31] have shown for several binary blends that Eq. (5) is valid for $\phi_{PT} \le \phi \le 1$; hence, E_{0i} ($i=1, 2$) can be evaluated from Eq. (5). Making $E=E_i$ and $\phi=1$ in Eq. (5) gives $E_{0i} = E_i(1-\phi_{PT,i})^{-\beta}$, where E_i is the modulus of pure component i. Whenever $E_1 \gg E_2$ (which is the case studied here), the EBM predicts that $E=E_1\phi_{p1}$. These expressions

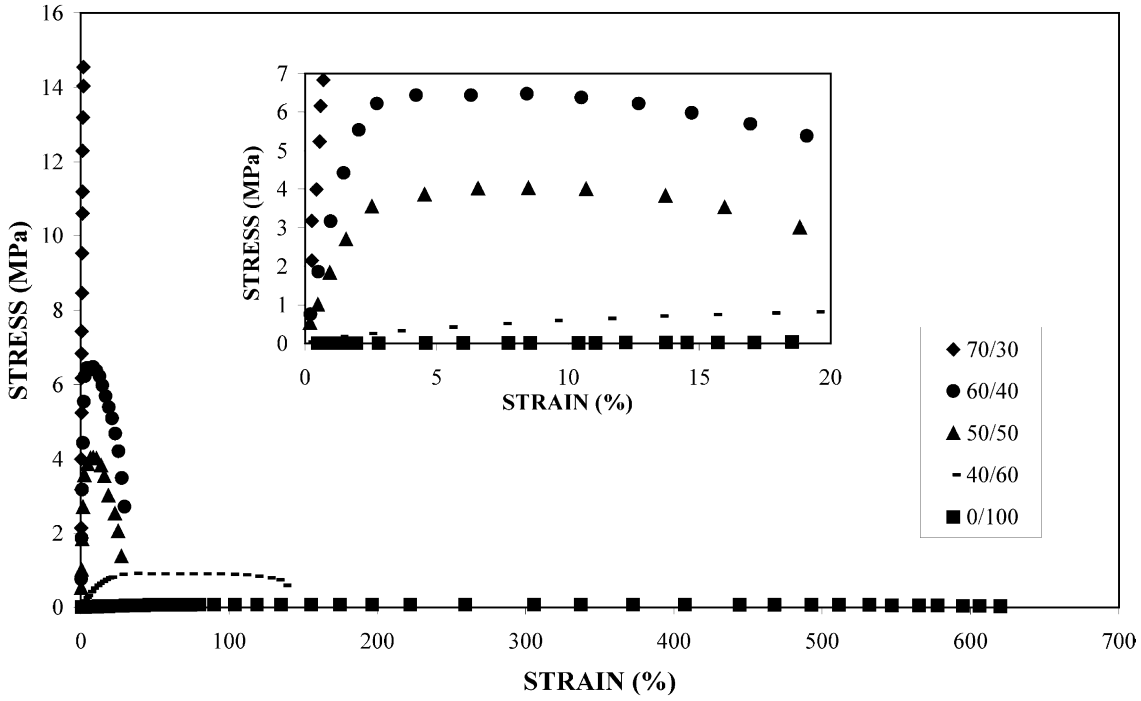

Fig. 2. Stress–strain data for PSt-core/PBA-shell polymers with different PSt/PBA ratios.

allow the calculation of the parallel and series contributions of the volume fractions as follows:

$$\phi_{pi} = \left(\frac{\phi_i - \phi_{PT,i}}{1 - \phi_{PT,i}}\right)^{\beta i}; \quad \phi_{si} = \phi_i - \phi_{pi}\ (i = 1, 2) \qquad (6)$$

The predictions of the EBM were done using the universal constants ($\phi_{PT,i}=0.156$ and $\beta_i=1.833$ for $i=1, 2$) and the experimental modulus of the homo-polymers measured in our laboratory. Predictions agree well with experimental tensile modulus of the soft-core/hard-shell for $\phi_{PSt} \geq 0.4$

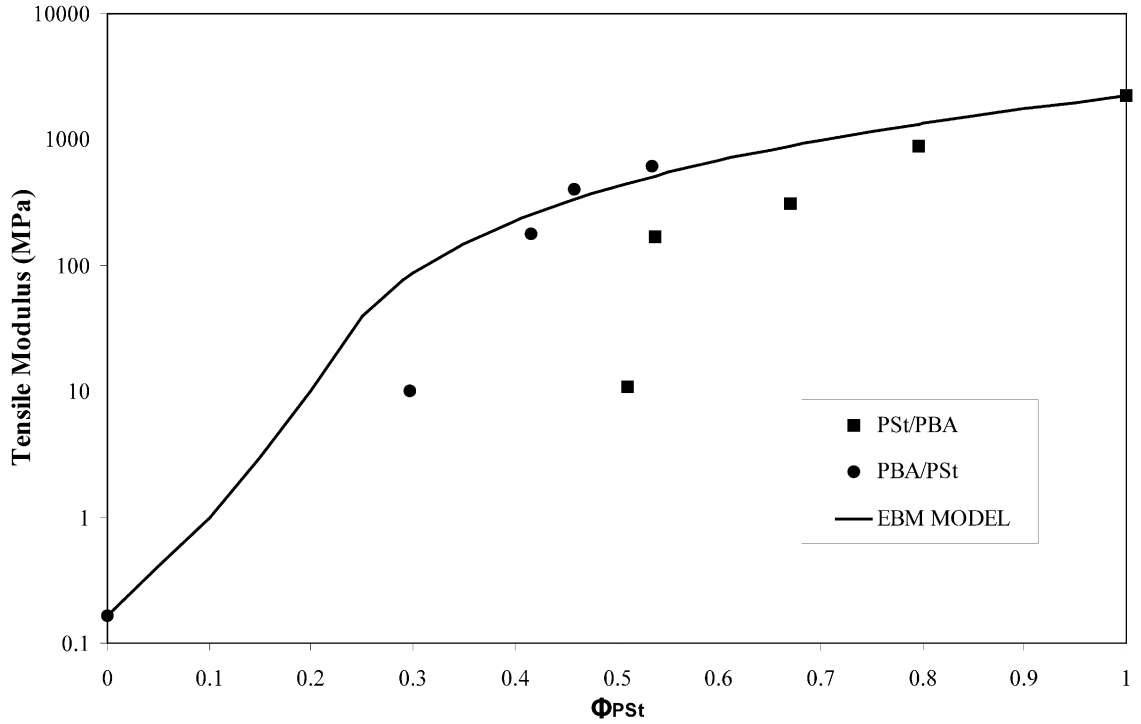

Fig. 3. Tensile modulus versus PSt volume fractions for PBA-core/PSt-shell (●) and PSt-core/PBA-shell (■) polymers. Solid line represents the predictions of the equivalent box model.

(Fig. 3). For lower values the data depart from model predictions. On the other hand, experimental modulus of the hard-core/soft-shell polymers deviates considerably from the predictions of the model (Fig. 3). In this case, the experimental data fall below the predictions and deviations become larger as the PSt content diminishes. Incidentally, much better fitting can be obtained (not shown) by using higher $\phi_{PT,I}$ and β_I values, but within the reported experimental range, $0.1 < \phi_{PT} < 0.22$ and $1.7 < \beta < 1.9$ [32].

Inasmuch as the EBM model do not takes into account which polymer is forming the continuous (matrix) phase, another model was employed to test the data and find out whether inversion could have occurred during the formation and/or processing of the core/shell materials. The Kerner model was chosen because it predicts the modulus of an emulsion blend with either component as the continuous phase [33]. The Kerner equation is given by [15]:

$$E = E_c \frac{\phi_d E_d}{(7-5\upsilon_c)E_c + (8-10\upsilon_c)E_d} + \frac{\phi_c}{15(1-\upsilon_c)} \Big/ \frac{\phi_d E_c}{(7-5\upsilon_c)E_c + (8-10\upsilon_c)E_d} + \frac{\phi_c}{15(1-\upsilon_c)} \quad (7)$$

Here the sub-indexes ‘c’ and ‘d’ refer to the continuous and the disperse phase, respectively, and υ_c stands for the Poisson ratio of the continuous phase.

Fig. 4 depicts the comparison between experimental data for both soft-core/hard-shell and hard-core/soft shell polymers and the predictions of Eq. (7) assuming that either PSt or PBA is the continuous phase. The predictions assuming that PSt is the continuous phase agree well with the PBA/PSt core/shell materials with $\phi_{PSt} \geq 0.4$. For lower volume fractions, Eq. (7) over-predicts the modulus. On the other hand, with the assumption that PBA is the continuous phase in the PSt/PBA core/shell polymers, the model predictions deviate substantially from the experimental values, Notice, however, that the data tend to approach the Kerner model predictions with the assumption that PSt is the continuous phase. These results suggest that a phase inversion or a disruption of the core/shell structure may occur when PBA is ‘forming’ the shell, i.e. in the PSt/PBA core/shell polymers.

To investigate further this issue, we applied the theory of Sundberg et al. [34], in which the thermodynamically preferred morphology is the one with a minimum interfacial free energy change among four possible equilibrium morphologies, namely, core/shell, inverted core/shell, individual particles and hemisphere. Details of the derivation of the equation used to estimate the interfacial free energy change ($\Delta\gamma$) of the different morphologies are given elsewhere [35]. The equations for $\Delta\gamma$ for each of the cases are the following:

$$(\Delta\gamma)_{CS} = \gamma_{12} + \gamma_{2w}(1-\phi_2)^{-2/3} - \gamma_{1w} \quad (8)$$

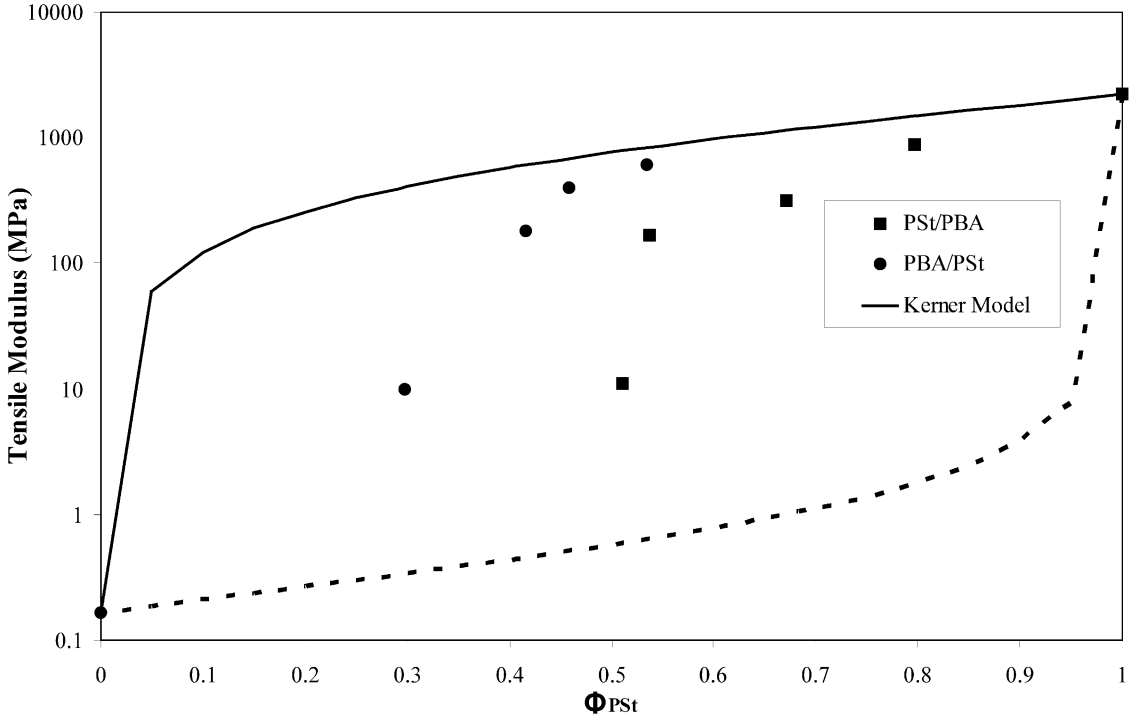

Fig. 4. Tensile modulus versus PSt volume fraction fractions for PBA-core/PSt-shell (●) and PSt-core/PBA-shell (■) polymers. Predictions of the Kerner model assuming that PSt (solid line) or PBA (dashed line) is the continuous phase.

$$(\Delta\gamma)_{ICS} = \gamma_{1w}[(1-\phi_2)^{-2/3} - 1] + \gamma_{12}[\phi_2/(1-\phi_2)]^{2/3} \quad (9)$$

$$(\Delta\gamma)_{IP} = \gamma_{2w}\left[\frac{\phi_2}{(1-\phi_2)}\right]^{2/3} \quad (10)$$

In these equation, the sub-indexes CS, ICS and IP stand for core/shell, inverted core/shell and individual particles, respectively, whereas the sub-indexes 1, 2 and w stand for polymers 1 and 2, and water. Here, polymer 1 is the one forming the original seed.

The calculations of the interfacial tension at the temperature of reaction (60 °C) required for the calculations were estimated from thermodynamic data taken from the literature [35,36] and the harmonic mean equation, given by [35]:

$$\gamma_{jk} = \gamma_j + \gamma_k - \frac{4\gamma_j^d\gamma_k^d}{\gamma_j^d + \gamma_k^d} - \frac{4\gamma_j^p\gamma_k^p}{\gamma_j^p + \gamma_k^p} \quad (j,k = 1,2 \text{ or w}) \quad (11)$$

Here γ_{jk} is the interfacial tension of the pair (j, k), γ_j is the surface tension of phase j(=1, 2 or w), γ^d and γ^p are the dispersive and polar components of the surface tension. The surface tension of water was taken as equal to that of an aqueous solution of DTAB at 20 °C, measured in our laboratory. The thermodynamic parameters required and the estimated interfacial tensions of the pairs involved are reported in Table 4.

Table 5 summarizes the calculations of the interfacial free energy change for the three morphologies considered and the different compositions of the core/shell examined. When PBA forms the seeds, the minimum interfacial free energy change corresponds to the core/shell structure, i.e. the PSt incorporates over the seeds. This PBA-core/PSt-shell morphology is confirmed by TEM, where the dark domains correspond to PSt and the light domains to PBA (Fig. 5). Moreover particle size estimated from TEM is similar to that measured by QLS. However, when PSt forms the seeds, the minimum interfacial free energy change corresponds to the inverted core/shell structure, so phase inversion should occur. Fig. 6 shows that in this case also the PSt (dark domains) is in the outer layer, although incomplete inverted core/shell morphology is observed. Hence, we have to conclude, based on this analysis and TEM observations, that PSt is mainly located in the shell of these materials notwithstanding the order of addition of the monomers during the preparation of the core/shell structure. However, the mechanical properties of polymers with similar weight ratio of PSt and PBA depend on the order of addition, which suggests that the inversion may not be complete. In fact, Okubo [37] reported that the resulting morphology depends on, among other factors, on the mode of addition of the second monomer (monomer absorption versus dropwise method) over the seed and aging. Okubo suggested that the monomer absorption method tends to give incomplete inversion (when inverted core/shell structures are thermodynamically favored) due to lack of enough time for diffusion and the high viscosity of the reacting medium. Hence, it is likely that incomplete inversion occurred for the PSt/PBA particles, which can explain the lower mechanical properties compared to the 'thermodynamically favored' PBA/PSt particles. Indeed, Fig. 6 confirms that incomplete inversion occurs.

Table 5
Interfacial free energy changes for different morphologies of the different core/shell compositions prepared here

Core/shell composition	$(\Delta\gamma)_{CS}$ (mN/m)	$(\Delta\gamma)_{ICS}$ (mN/m)	$(\Delta\gamma)_{IP}$ (mN/m)	Predicted morphology
PSt/PBA 70/30	7.96	3.85	9.21	ICS
PSt/PBA 60/40	8.56	4.44	10.21	ICS
PSt/PBA 50/50	16.00	11.62	20.77	ICS
PSt/PBA 40/60	17.22	12.78	22.33	ICS
PBA/PSt 70/30	3.93	6.86	11.33	CS
PBA/PSt 60/40	7.29	11.02	19.84	CS
PBA/PSt 50/50	8.95	12.83	18.0	CS
PBA/PSt 40/60	11.99	16.79	21.5	CS

The EBM can also be used to predict the tensile strength of two-component, phase-separated polymeric systems. The predictions of Eq. (4), using again the values of $\phi_{PT}=0.153$ and $\beta=1.833$ for both component polymers, and the experimental tensile strengths of both types of core/shell polymers are shown in Fig. 7. As expected, the yield (or ultimate) strength increases as the PSt content in both types of core/shell polymers is increased; moreover, the tensile strength of PBA-core/PSt-shell polymers is consistently

Table 4
Thermodynamic properties of polystyrene, poly(butyl acrylate) and water for surface tension calculations

Substance	γ (mN m^{-1})$\vert_{20\ °C}$	dγ/dT (mN m °C^{-1})	$\chi^p=\gamma^p/\gamma$
PBA	33.7[a]	0.070[a]	0.098[a]
PSt	40.7[a]	0.070[a]	0.168[a]
Water	39.5[b]	0.228[a]	0.696[a]

[a] Values taken from Refs. [35,36].
[b] Value corresponds to the surface tension of an aqueous solution of CTAB measured at 20 °C.

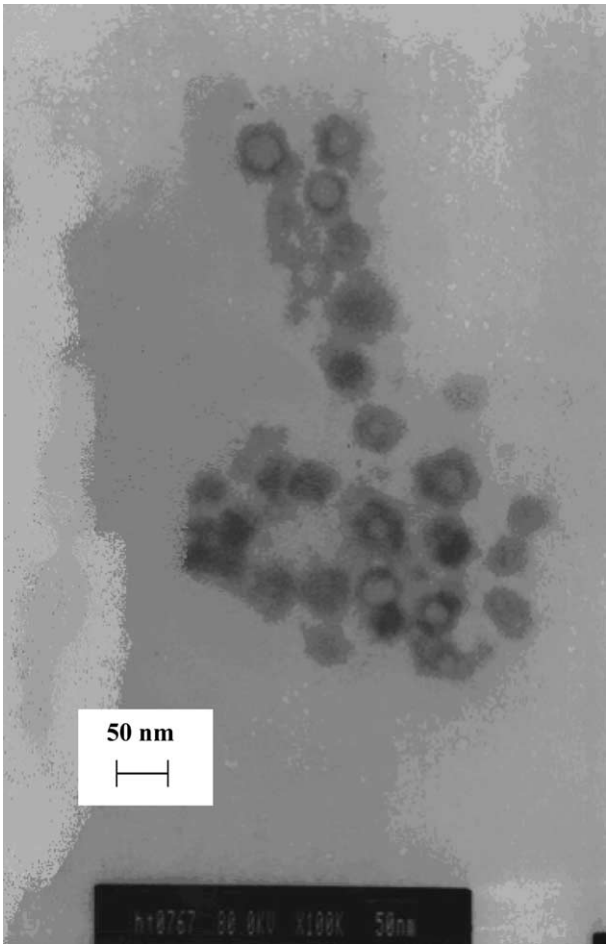

Fig. 5. TEM photography of PBA/PSt core/shell polymer particles.

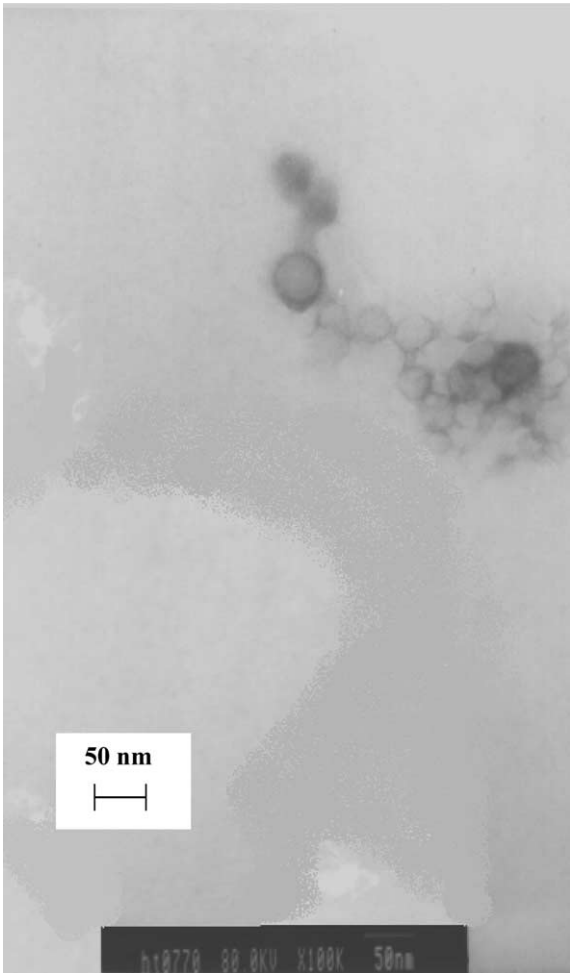

Fig. 6. TEM photography of PSt/PBA core/shell polymer particles.

larger than those of the PSt-core/PBA-shell polymers presumably because of the proposed incomplete phase inversion occurring in the later particles. Then, as expected, the predictions of the EBM model follow closely the experimental data for the soft-core/hard-shell polymers but they over-predict the data for the hard-core/soft-shell polymers.

Hardness and impact energy results for both types of core/shell polymers are shown in Table 6. Due to its rubbery nature, poly(butyl acrylate) does not break in the impact test. As expected, the hardness increases and impact energy decreases with increasing PSt content, regardless of its location, the tensile modulus (E), the ultimate elongation, tensile stress, impact energy and hardness of the core-shell materials are summarized in Table 6.

4. Concluding remarks

In this work we demonstrated that is possible to obtain core-shell polymers of polystyrene/poly(butyl acrylate)

Table 6
Hardness shore A and impact energy of core-shell polymers

Core/shell composition	Young Modulus (MPa)	Ultimate Strain (%)	Tensile Stress (MPa)	Hardness Shore A	Impact energy (J/cm)
PSt/PBA 70/30	877.2	1.9	14.6	95.8	0.09
PSt/PBA 60/40	312.5	29.5	6.5	92.2	0.27
PSt/PBA 50/50	166.7	22.9	4.4	81.0	1.19
PSt/PBA 40/60	10.9	137.3	0.6	59.2	24.02
PBA/PSt 70/30	10.0	73.3	1.4	60.8	14.34
PBA/PSt 60/40	178.6	54.5	7.2	83.7	11.9
PBA/PSt 50/50	401.6	33.0	13.5	85.7	1.14
PBA/PSt 40/60	606.1	1.7	9.5	91.0	0.7
PBA/PSt 0/100	2200.0	0.9	36.5	96.0	0.05

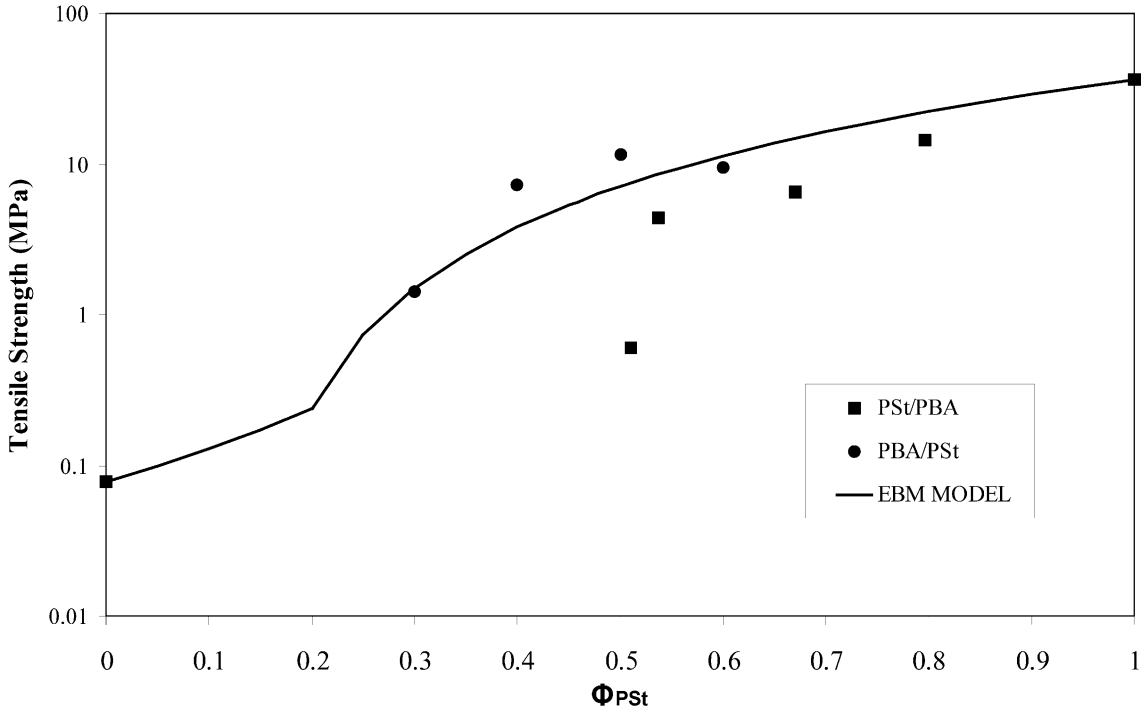

Fig. 7. Tensile strength versus PSt volume fractions for PBA-core/PSt-shell (●) and PSt-core/PBA-shell (■) polymers. Solid line represents the predictions of the equivalent box model.

with high solid content by a two-stage microemulsion polymerization. This process is similar to the traditional emulsion polymerization for making core-shell polymers at industrial level.

Elsewhere we reported that PSt-core/PBA-shell polymers made by microemulsion polymerization were tougher and with similar elongations at break than emulsion-made polymers of similar composition [16]. Here we examined the mechanical properties of core-shell PSt/PBA polymers as a function of composition and location of the soft and brittle polymers. Our results indicate that by varying the core-shell composition and the initial location of the polymers, it is possible to obtain materials with a broad range of mechanical properties. These polymer particles are promising for using in coatings, adhesives or impact-resistance plastics due to their mechanical characteristics and small sizes.

Acknowledgements

This work was supported by the Consejo Nacional de Ciencia y Tecnología (Grant # 38725-U). S. López-Cuenca also acknowledge scholarships from CONACYT. JE Puig thanks the Ministerio de Educación y Ciencia of Spain for support.

References

[1] Rios L, Hidalgo M, Cavaille JY, Guillot J, Guyot A, Pichot C. Colloid Polym Sci 1991;269:812–24.
[2] Lee S, Rudin A. In: Daniels E, Sudol Ed, El-Aasser MS, editors. Polymer latexes. ACS symposium series, 492, 1992. p. 234.
[3] Hidalgo M, Cavaille JY, Cabane B, Chevalier Y, Guillot J, Rios L, et al. Polym Adv Technol 1995;6(5):296–300.
[4] Lu M, Keskkula H, Paul DR. Polymer 1996;37:125–35.
[5] Nelliappan V, El-Aasser MS, Klein A, Daniels ES, Roberts JE, Pearson NA. J Appl Polym Sci 1997;65:581–93.
[6] Hidalgo M, Cavaille JY, Guillot J, Guyot A, Pichot C, Rios L, et al. Colloid Polym Sci 1992;270:1208–21.
[7] Mendizábal E, Hernández-Patiño PJ, Puig JE, Canché-Escamilla G, Katime I, Castaño V. J Appl Polym Sci 1999;74(14):3299–304.
[8] Wang GJ, Klang CS, Jin RG. Prog Org Coat 2004;50(1):55–61.
[9] Qian JY, Pearson RA, Dimonie VL, El-Aasser MS. J Appl Polym Sci 1995;58(2):439–48.
[10] El-Aasser MS, Hu R, Dimonie VI, Sperling LH. Colloid Surf A 1999; 153(1–3):241–53.
[11] Ha JW, Park IJ, Lee SB, Kim DK. Macromolecules 2002;35(18): 6811–8.
[12] Ferguson CJ, Russell GT, Gilbert RG. Polymer 2002;43(24): 6371–82.
[13] Kalinina E, Kumacheva E. Macromolecules 2001;34(18):6380–6.
[14] Kalinina E, Kumacheva E. Chem Mater 2001;13(1):35–8.
[15] Robeson LM, Berner RA. J Polym Sci, Part B: Polym Phys 2001;39: 1093–106.
[16] Aguiar A, Gonzalez-Villegas S, Rabelero M, Mendizábal E, Puig JE. Macromolecules 1999;32(20):6767–71.
[17] Puig JE. In: Salamone JP, editor. Polymeric materials encyclopedia, vol. 6. Boca Raton: CRC press; 1996. p. 4333–41.

[18] Candau F. In: Kumar P, Mittal KL, editors. Handbook of microemulsion science and technology. New York: Marcel Dekker; 1999. p. 679–712.
[19] Capek I. Adv Colloid Interf Sci 1999;80(2):85–149.
[20] Candau F. In: Paleos CM, editor. Polymerization in organized media. Philadelphia: Gordon Breach Science Publishers; 1992.
[21] Puig JE. Rev Mex Fis 1999;45:18.
[22] Rabelero M, Zacarías M, Mendizábal E, Puig JE, Domínguez JM, Katime I. Polym Bull 1997;38:695–700.
[23] Ming W, Jones FN, Fu S. Polym Bull 1998;40(6):749–56.
[24] Ming W, Jones FN, Fu S. Macromol Chem Phys 1998;199(6):1075–9.
[25] Xu XJ, Chew CH, Siow KS, Wong MK, Gan LM. Langmuir 1999; 15(23):8067–71.
[26] Sosa N, Peralta RG, López RG, Ramos LF, Katime I, Cesteros C, et al. Polymer 2001;42(16):6923–8.
[27] Hu R, Dimonie VL, El-Aasser MS. J Appl Polym Sci 1997;64: 1123–34.
[28] Kolarik J. Polymer 1994;35(17):3631–7.
[29] Kolarik J. Polymer 1996;36(20):2518–24.
[30] DeGennes PG. J Phys Lett (Paris) 1976;37:L1.
[31] Lyngaae-Jorgersen J, Kuta A, Sondergaard K, Poulsen KV. Polym Networks Blends 1993;3(1):1–13.
[32] Utracki L. J Rheol 1991;35(8):1615–37.
[33] Kerner EH. Proc Phys Soc London Sect B 1956;69B:808–13.
[34] Sundberg DC, Casassa AP, Pantazopoulos J, Muscato MR. J Appl Polym Sci 1990;41:1425–42.
[35] Zhao K, Sun P, Liu D, Wang L. J Appl Polym Sci 2004;92:3144–52.
[36] Huo D, Liu D. Polym Int 2002;51(7):585–93.
[37] Okubo M. Makromol Chem Macromol Symp 1990;35/36:307.